COLD GAS DYNAMIC SPRAYING OF METAL MATRIX COMPOSITE COATINGS WITH SUBSEQUENT FRICTION STIR PROCESSING

Tom Peat, University of Strathclyde, Glasgow, United Kingdom

Alexander Galloway, University of Strathclyde, Glasgow, United Kingdom
Athanasios I. Toumpis, University of Strathclyde, Glasgow, United Kingdom
Philip McNutt, TWI, Cambridge, United Kingdom
Naveed Iqbal, TWI, Rotherham, United Kingdom

SYNOPSIS

The present study forms an initial investigation in to the development of an innovative process to apply wear resistant surface layers to a chosen substrate material. Tungsten carbide – cobalt chromium, chromium carbide – nickel chromium and aluminium oxide coatings were cold spray deposited on to AA5083 grade aluminium and subsequently friction stir processed. In order to improve the deposition efficiency of the cold spray process, coatings were co-deposited with powdered AA5083. Friction stir processing (FSP) has been used in combination with the cold spray deposited coating to produce an engineered surface layer containing evenly dispersed reinforcing particles that reflects the constituent phases of the feedstock powder. Microstructural characterisation was performed on the test specimens making use of micro-hardness testing, light optical and scanning electron microscopy with electron dispersive spectroscopy to establish the elemental composition of the processed layer. The resulting data was contrasted with as-deposited coatings (no FSP) to highlight the variation in microstructure between the two conditions.

The results demonstrate that FSP has improved the dispersal of reinforcing particles within the metal matrix composite layer with the average interparticle spacing decreasing by up to 68%. The micro-hardness of friction stir processed material shows an increase of approximately 540% over the unaltered substrate and 118% increase over the as-deposited MMC layer, in the case of the tungsten carbide reinforced coating.

1. INTRODUCTION

Cold-gas dynamic spraying (CGDS) is a thermal spraying process used to deposit coatings on to a variety of substrate materials through the acceleration and impingement of feedstock powder particles [1,2]. In contrast with many other commercially available thermal

spraying technologies such as high velocity oxy-fuel (HVOF) [3] or plasma spray [3], the temperatures in CGDS never exceed the melting point of the powder particles. In doing so, the deposited coating retains the phase composition of the feedstock material [2]. Particle adhesion to the substrate material is achieved through the severe plastic deformation of impinging particles that occurs due to the high particle impact velocities generated by the cold spray system. The low temperatures allow the technique to be applied to materials with low melting points such as aluminium or magnesium. This is of particular interest to the automotive and aerospace industries who look to optimise components for minimal weight whilst maintaining strength and wear performance [4].

Deposition of wear resistant coatings, particularly cermet materials such as tungsten carbide or chromium carbide is difficult to achieve due to the limited deformability of ceramic particles at the low temperatures experienced during CGDS [5]. The presence of carbide particles within the feedstock powder results in minimal deformation upon contact with the surface of the substrate, with existing studies reporting a grit blasting effect from the impinging carbide particles [6,7]. Minimal deformation upon impact can also result in porosity within the coating layer which will reduce its associated wear resistance [8]. The addition of a ductile metallic binder has been shown to enhance the deposition rate of ceramic coatings [9], with the metallic binder typically being incorporated as agglomerated-sintered particles or by mixing cermet and binder powders prior to spraying.

Friction stir processing (FSP) has been shown by Morisada et al. [10] to reduce the presence of defects within a thermally sprayed cermet coating [10]. The authors also report FSP to refine and distribute the carbide particles within the deposited layer. FSP is a form of solid-state surface modification that makes use of a rotating tool that is plunged into a chosen substrate and traversed along a pre-defined path referred to as the processing track. Contact between the rotating tool shoulder and substrate causes substantial heat generation softening the substrate material without reaching the melting point. The rotating motion forces material from the leading edge around to the rear of the tool where it is consolidated. Reported benefits of the FSP process include the removal of defects, homogenous dispersion of impurities and grain refinement within the stir zone [11].

The present study seeks to evaluate the application of FSP to CGDSed metal matrix composite (MMC) coatings that have been co-deposited using a twin powder feed system. Microstructural examination of coatings in the pre- and post-FSP conditions was carried out in order to highlight the effect of FSP on the structure of the MMC coatings. The quantity and distribution of cermet particles was measured in addition to the micro-hardness across the width

of the stir zone. The aim of the study was to assess the impact of FSP on a cold spray deposited coating, specifically to determine if FSP was capable of improving the distribution of reinforcing particles within the substrate matrix. The outcomes of this study will form a proof of concept for future development of this new technology titled “SprayStir”.

2. METHODOLOGY

2.1 Specimen Production

2.1.1 Cold spray deposition

In this study, commercially available tungsten carbide (WC-CoCr), chromium carbide (Cr_3C_2-NiCr) and aluminium oxide (Al_2O_3) powders were co-deposited with AA5083 powder on 6 mm AA5083 plates using a CGT GmbH Kinetiks 4000 CGDS system. The composition of feedstock powders can be found in Table 1, with the particle morphology exhibited in Fig. 1. The WC-CoCr and Cr_3C_2-NiCr particles are spherical in shape and are comprised of nano-scale tungsten carbides evenly distributed throughout a cobalt matrix. Al_2O_3 particles are comparably larger, are faceted and possess no metallic binder. The average particle size for each powder is indicated in Table 1.

Table 1. Powder composition

Coating Material	Powder Identification Code	Composition (wt.%)	Average Particle Size (µm)
WC-CoCr	Woka 3652	80.6W - 10Co - 4Cr - 5.2C - 0.2Fe	27.37
Cr_3C_2-NiCr	Woka 7202	69.9Cr - 20Ni - 9.6C - 0.5Fe	24.31
Al_2O_3	Al-1110-HP	100Al_2O_3	75.81

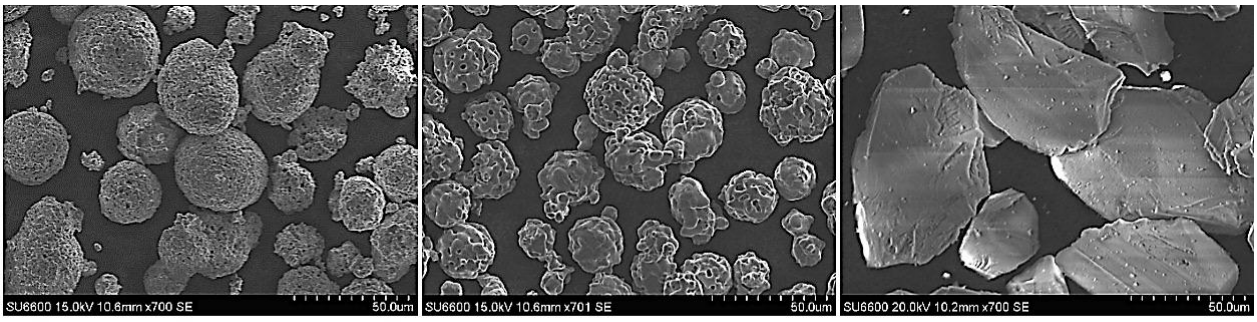

Fig. 1 Scanning electron micrographs of feedstock powder particles [x700]. a) WC-CoCr, b) Cr_3C_2-NiCr, c) Al_2O_3

Spraying was carried out using a conventional de Laval type nozzle at stand-off distance of 50 mm from the substrate, using nitrogen gas at a temperature of 500^{O}C. The spray system

was attached to an OTC 6 axis robotic arm in order to improve the repeatability of coating deposition. Following initial parameter development work, powders were sprayed using two 4000 series powder feeders, in the ratio 60% reinforcing material to 40% binder. This resulted in a coating thickness in the range 0.38 - 0.44 mm following the deposition of three layers (3 passes with the spray gun). The increased deposition efficiency of Cr_3C_2-NiCr resulted in a coating thickness of approximately 0.68 mm with three passes and as a result, only two passes were required for this coating. In order to provide a uniform surface for the FSP, coatings were milled to an optimal thickness of 0.3 mm.

2.1.2 Friction stir processing

FSP of coated specimens was carried out using a TTI precision spindle friction stir welding/processing machine. The tool was produced from H13 grade tool steel and featured a concave shoulder with 2 mm pin length. A drawing of the tool can be seen in Fig. 2. Initial development work on uncoated aluminium was carried out to establish appropriate machine parameters that were capable of producing processed tracks with no voids and minimal flash. For the processing of coated specimens it was necessary to incorporate a 3^{O} lead angle to the traverse direction to prevent the coating layer from being removed by the tool. The specific FSP parameters used throughout this study are included in Table 2. The quoted plunge depth is measured from the tip of the tool probe. A macroscopic image showing the cross section of a SprayStirred specimen is included in Fig. 3 and highlights the various regions within the stir zone that will be discussed throughout this paper.

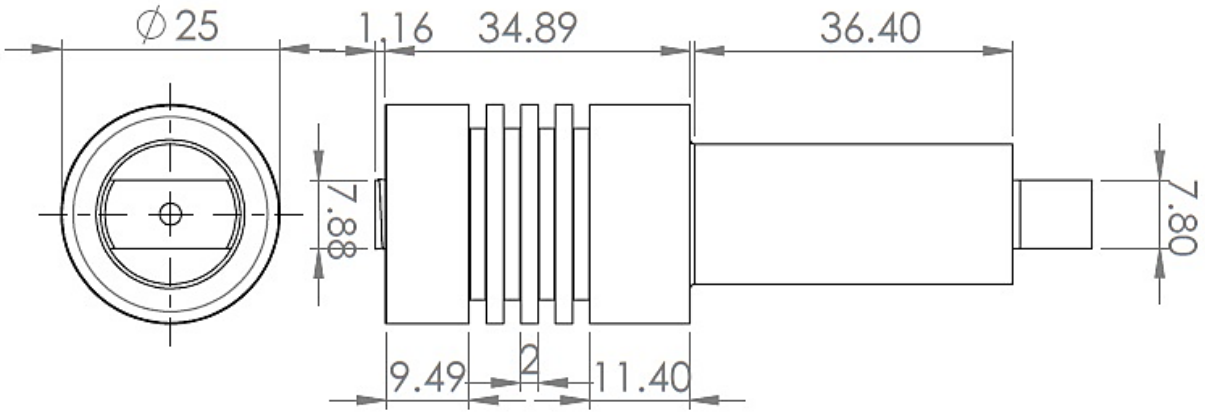

Fig. 2 Two dimensional technical drawing of the H13 FSP tool.

Table 2. FSP parameters

Tool Type	Pin Length (mm)	Rotation Speed (RPM)	Traverse Speed (mm/min)	Plunge Depth (mm)	Tilt Angle (^{O})
H13 Concave shoulder	2	600	272	3.8	3

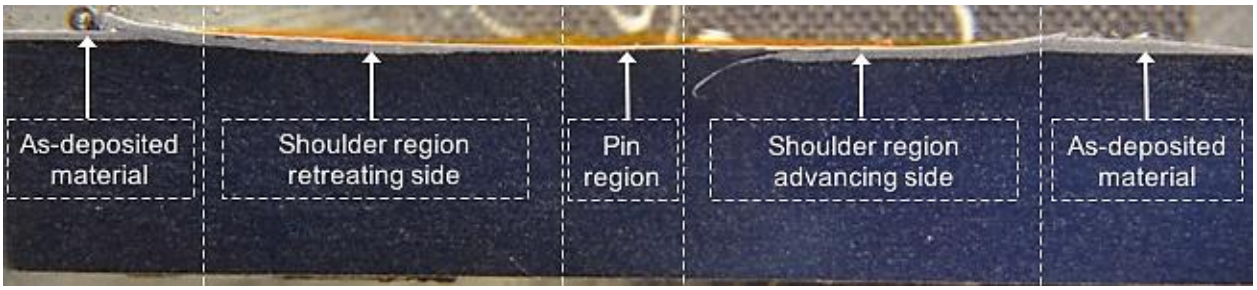

Fig 3. Macroscopic cross section of the stir zone from SprayStirred WC-CoCr.

2.2 Experimental Procedure

The following testing programme was implemented to achieve the aims of this study:

- Specimen preparation: Standard metallographic preparation techniques were employed to prepare specimens to a 0.5 μm finish for microstructural examination.
- Light optical microscopy: Optical micrographs depicted the distribution of reinforcing particles within the aluminium matrix in the as-deposited and FSPed conditions. Suitable micrographs were captured with an Olympus G51X series optical microscope and used to establish the ratio of binder to reinforcing particle using image analysis software.
- Scanning electron microscopy (SEM): A Hitachi S-3700 series SEM was used to capture high resolution images showing the distribution of carbides/oxides within the matrix prior to, and following FSP. Using energy dispersive spectroscopy (EDS) (Oxford Instruments INCA), the positions of the constituent elements were mapped highlighting the dispersion of reinforcing particles throughout the aluminium matrix.
- Micro-hardness measurements: Micro-hardness values were recorded to show the change in average hardness following FSP and to determine the hardness of the coating at various points within the stir zone. Data was collected using a Mitutoyo MVK-G1 micro-hardness tester with applied load of 100 gf. The reported hardness of each region within the processed zone is an average of 5 measurements. Readings were taken in the as-deposited coating, on the advancing and retreating sides of the tool and in the centre of the stir zone.

3. RESULTS AND DISCUSSION

3.1 Characterisation of the as-deposited MMC coating

Prior to FSP, the cold spray coatings were sectioned and examined to highlight the microstructure in the as-deposited condition. A magnified cross section of the WC-CoCr coating is exhibited in Fig. 4a. The lack of defects in the coating has been attributed to the significant deformation experienced by the ductile binder upon contact with the surface of the substrate due to the high velocities in CGDS. Fig. 4a also depicts agglomeration of WC-CoCr particles, resulting in areas within the coating that are void of any reinforcing particles.

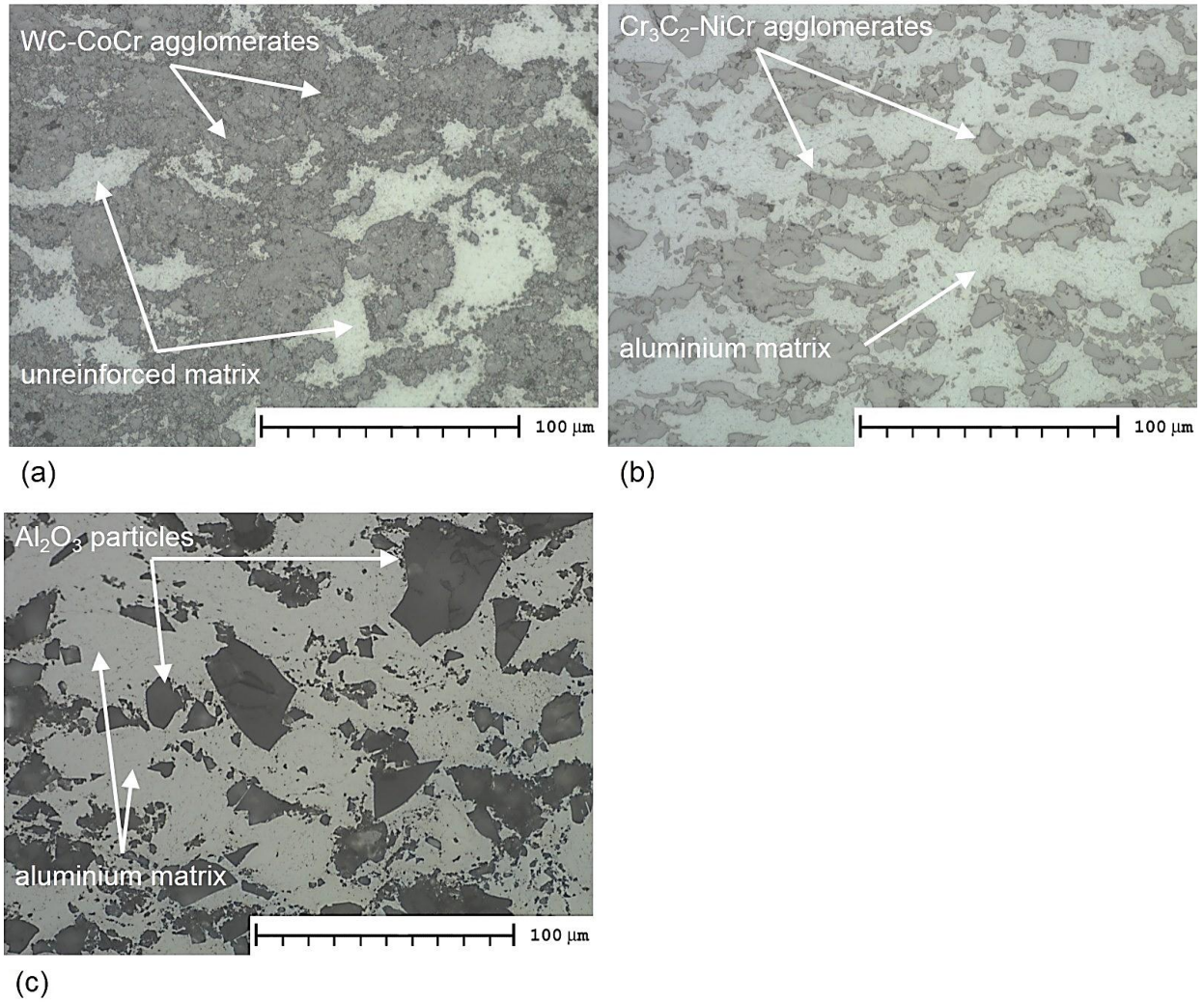

Fig 4. Light optical micrographs of the as-deposited region (Fig. 3). a) WC-CoCr, b) Cr_3C_2-NiCr, c) Al_2O_3 [x500 unetched]

Image analysis software determined that the coating comprises approximately 56% (vol.%) WC-CoCr and 44% binder. The measured value closely reflects the deposition ratio between the

metallic binder and reinforcing particles. Cr_3C_2-NiCr coating contains approximately 48% cermet material. The corresponding increase in vol.% of binder provides an explanation for the increase in coating thickness over WC-CoCr and Al_2O_3, with existing studies [9] also reporting increased deposition efficiency in the presence of higher quantities of ductile binder. Analysis of the Al_2O_3 coating revealed that the MMC contained approximately 60% binder to 40% oxide particles. Given that the quantity of binder is greater than in Cr_3C_2-NiCr it would be expected that deposition of Al_2O_3 would result in a greater coating thickness; however this was not the case. A study by Spencer et al. [4] attributed this to the rebounding of particles due to an inability to deform upon contact with the surface. This agrees with the recorded results given that both WC-CoCr and Cr_3C_2-NiCr powders contain inherent binder material in the form of cobalt and nickel, and as a result suffer greater deformation upon contact with other particles and with the surface of the substrate.

EDS was used to confirm that the dark grey regions observed in the optical micrographs represent the reinforcing particles, as opposed to pullout or contamination. Fig. 5 presents the distribution of tungsten, cobalt and aluminium within the MMC coating. The location of tungsten and cobalt aligns with the dark regions shown in the optical micrograph (Fig. 5b).

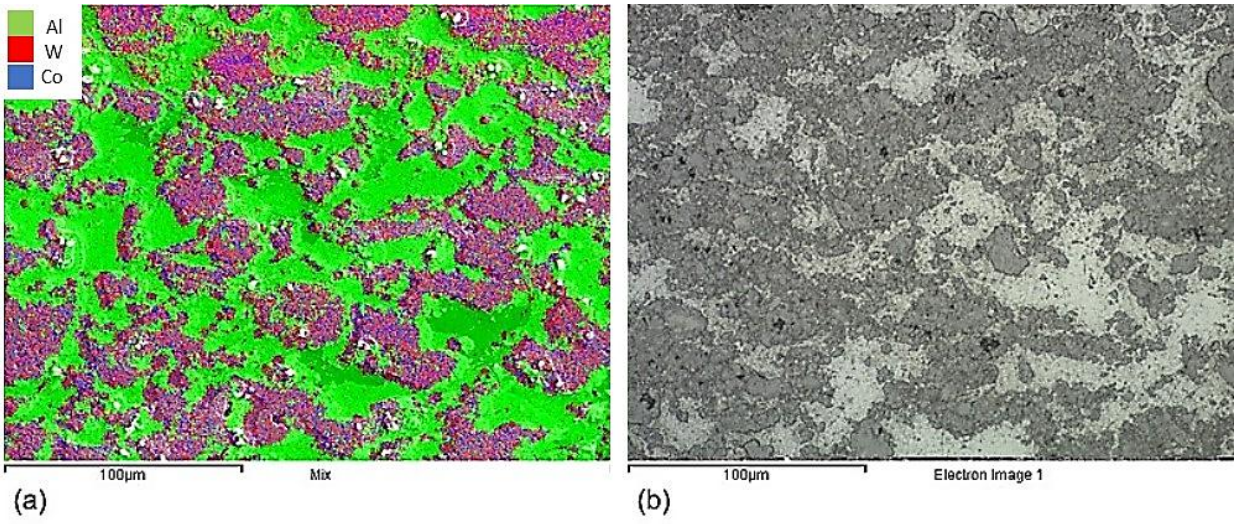

Fig 5. a) EDS image map showing distribution of tungsten and cobalt within the aluminium matrix, b) light optical micrograph of an equivalent region in the WC-CoCr coating [x500 unetched].

Micro-hardness measurements were taken on the as-deposited coatings highlighting the effect of the three different reinforcing particles on the average hardness (Fig. 6). The results show that the MMC containing WC-CoCr reinforcing particles exhibited the greatest average

hardness (239.6 Hv) with the MMC containing Al_2O_3 recording the lowest average hardness (183.2 Hv). The Al_2O_3 coating also features the greatest scatter of results owing to the lower quantity of Al_2O_3 particles within the aluminium matrix resulting in hardness indents being made on unreinforced substrate material. The results also demonstrate a correlation between increased hardness and greater quantities of reinforcing particles.

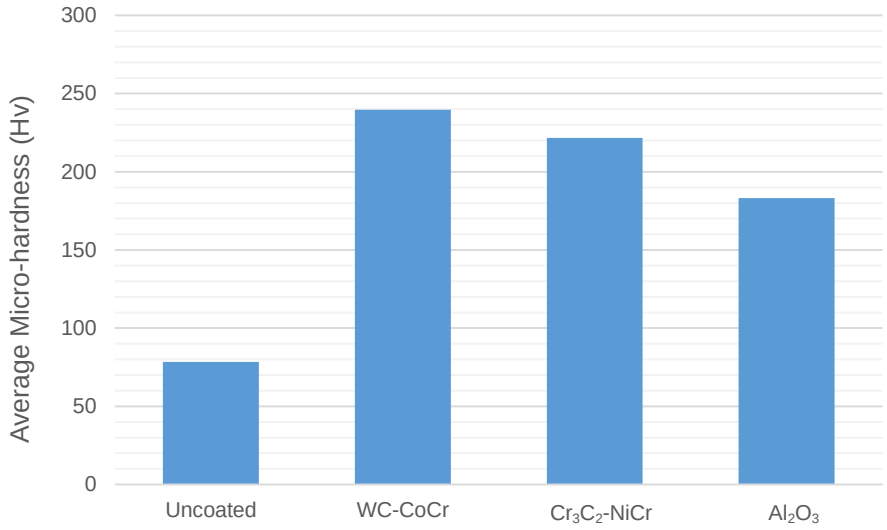

Fig 6. Average hardness values of the co-deposited MMC coatings.

3.2 Characterisation of SprayStirred MMC coatings

The as-deposited cold spray coatings depicted in Fig. 4 were exposed to FSP at 600 RPM resulting in the microstructures that can be observed in Fig. 7. FSP has caused significant refinement of the as-deposited particles and has removed the large agglomerates seen in Fig. 4a. Furthermore, the homogeneity of reinforcing particles throughout the aluminium matrix has been improved for all of the coating types.

In the case of Cr_3C_2-NiCr (Fig. 7b), the micrograph reveals increased particle refinement along the top of the image and corresponds to the region that is exposed to the greatest stirring from the tool shoulder [13]. The effects are also apparent in WC-CoCr and Al_2O_3 coatings with both demonstrating a greater level of particle refinement towards the top of the MMC layer. This feature is highlighted in Fig. 8. The level of refinement achieved with FSP is substantial, with few particles in the as-deposited condition remaining. Multiple FSP passes have been shown to increase the level of grain refinement by Ma et al. [14] and it is expected that additional FSP passes will result in further refinement of the reinforcing particles within the MMC.

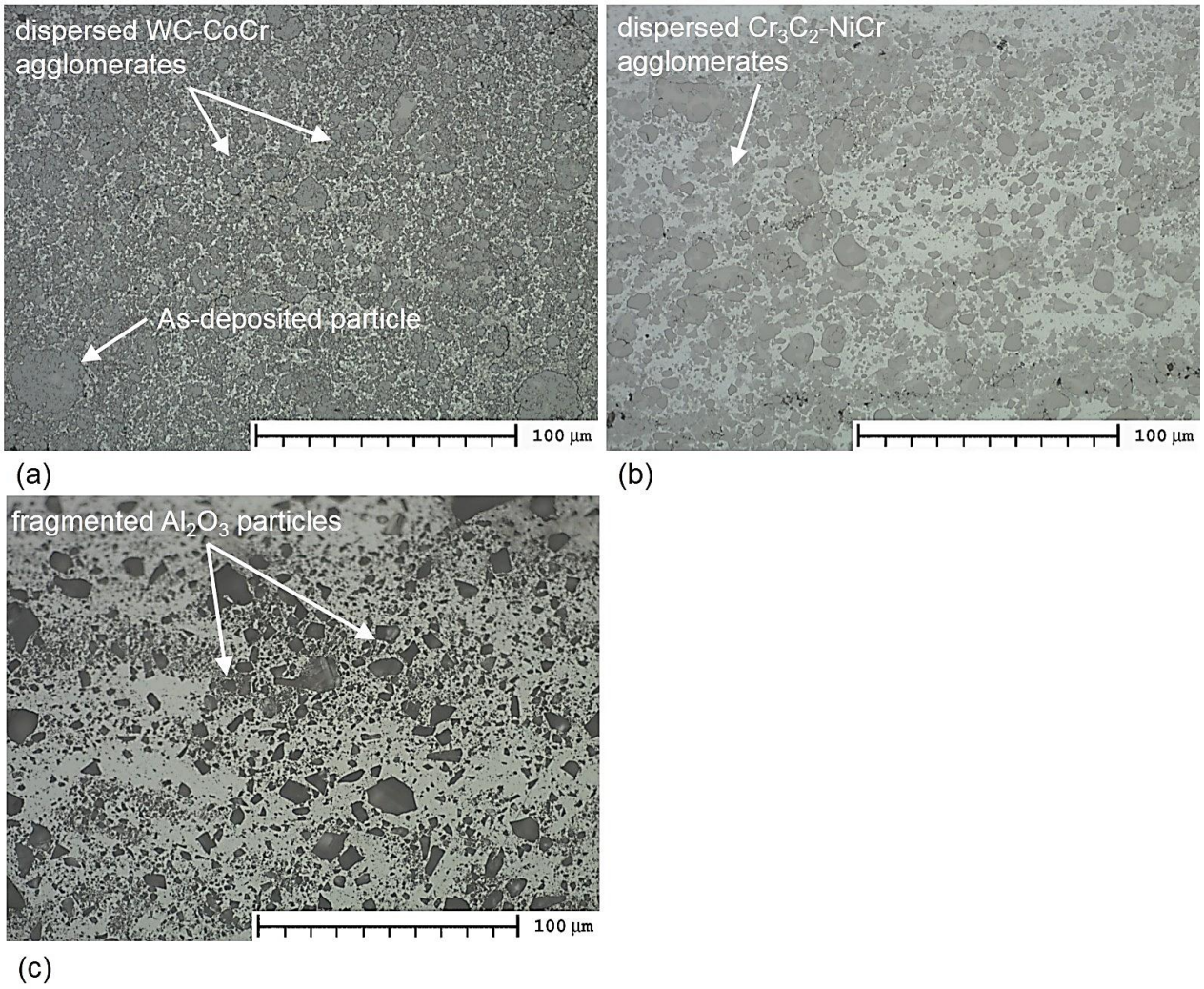

Fig 7. Light optical micrographs of retreating side of the tool (Fig. 3) showing the SprayStirred MMC coating with the dark reinforcement particles evenly dispersed throughout the light grey aluminium matrix. a) WC-CoCr [x500], b) Cr_3C_2-NiCr [x500], c) Al_2O_3 [x500].

The particle distribution post-FSP can be better observed in the EDS images depicted in Fig. 9. The images depict the location of the reinforcing particle within the matrix and highlight the dispersal of the large agglomerates following FSP. Fiedler et al. [15] noted that micro-reinforcement mechanisms, occur directly as a result of improved dispersion and reduced agglomerations. As demonstrated in Fig. 9, this has been achieved with the use of FSP on the deposited MMC. The wt.% of the various elements within the MMC coating was also recorded using EDS software with the results reported in Table 3.

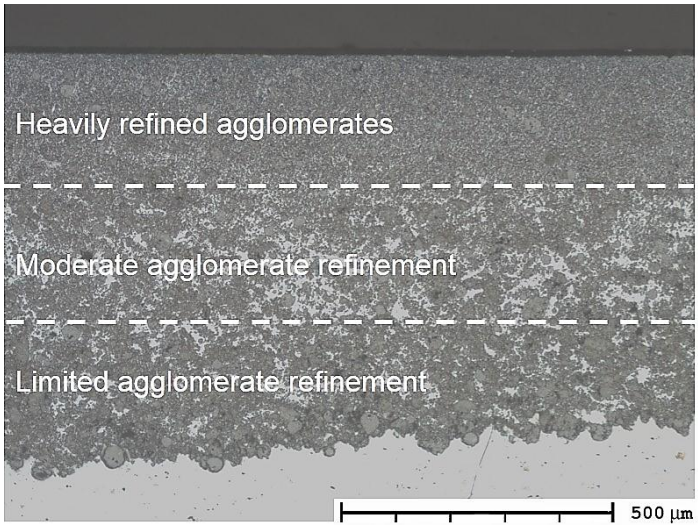

Fig 8. Optical micrograph highlighting the variation in particle refinement through the depth of the SprayStirred layer (Fig. 3).

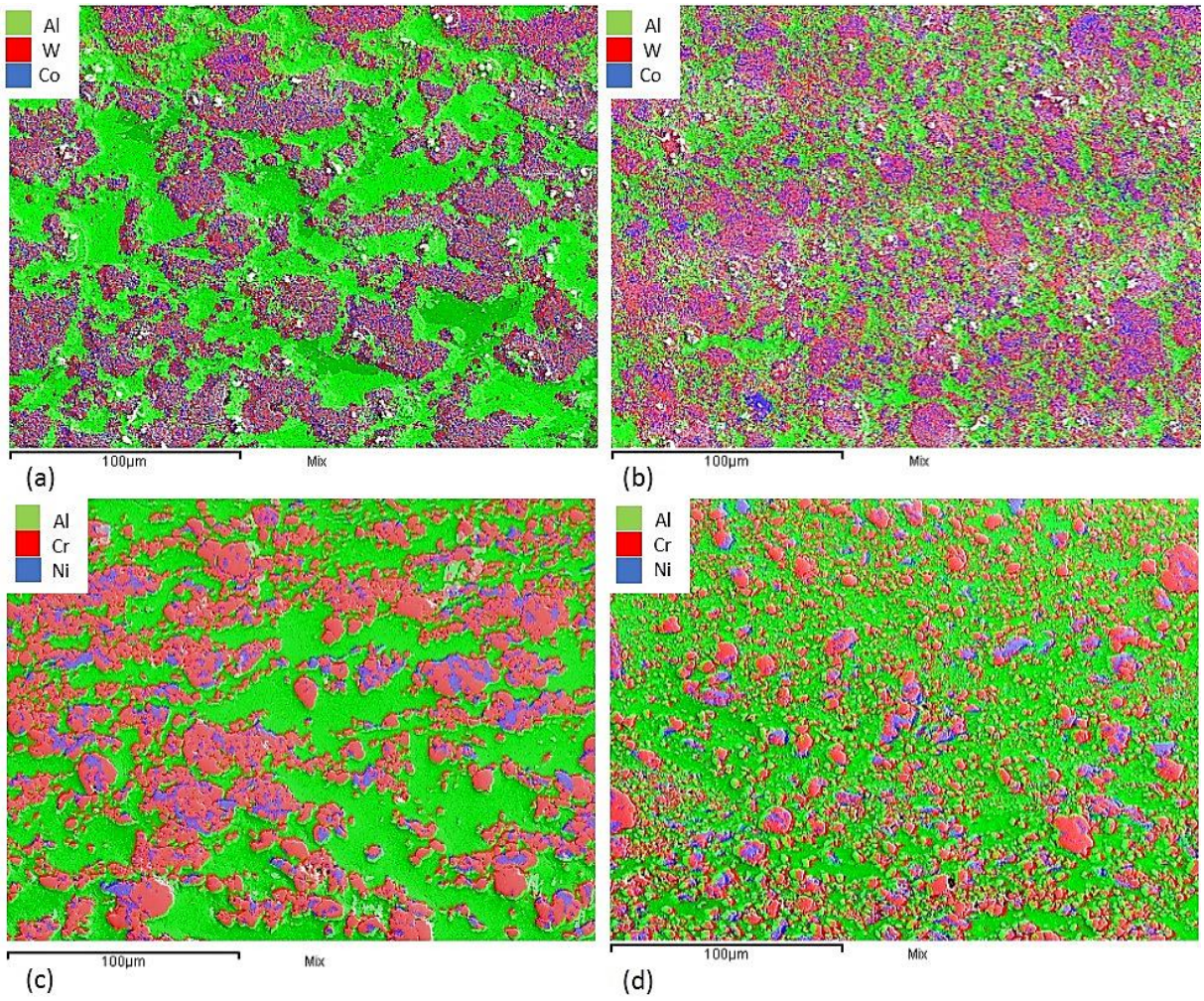

Fig 9. EDS mapping showing distribution of reinforcing particles [x500]. a) As-deposited WC-CoCr, b) SprayStirred WC-CoCr, c) As-deposited Cr_3C_2-NiCr, d) SprayStirred Cr_3C_2-NiCr

Table 3. EDS elemental analysis (wt.%)

		Mg	Al	Cr	Ni	Co	W	O
As-Deposited	WC-CoCr	1.51	32.22	2.54		5.54	58.19	
	Cr_3C_2-NiCr	2.06	39.52	42.92	15.51			
	Al_2O_3	2.60	86.06					11.35
SprayStirred (Retreating)	WC-CoCr	0.83	19.35	3.29		7.68	68.85	
	Cr_3C_2-NiCr	2.09	39.82	41.85	16.23			
	Al_2O_3	2.56	86.48					10.96
SprayStirred (Advancing)	WC-CoCr	1.54	33.79	2.78		5.95	55.95	
	Cr_3C_2-NiCr	2.23	49.51	36.34	11.92			
	Al_2O_3	2.84	90.4					6.67

The micro-hardness of coatings following FSP is presented in Fig. 10. Optical micrographs of the location in which the hardness indents have been made are also exhibited in the Fig. 11, to show the microstructure in the region surrounding the micro-hardness indents. The recorded data reveals a noticeable drop in the micro-hardness in the centre of the processed track. Analysis of this region reveals a lack of reinforcing particles and aligns with the path that the tool probe makes through the material. The lack of reinforcing particles in this region is attributed to the effects of the tool probe forcing reinforcing particles from the surface down to the base of the stir zone. The phenomenon can be seen in Fig. 12 and is present within all three MMC coatings.

Fig. 10 also presents the average hardness values for unaltered substrate and FSPed substrate (with no reinforcing particles). FSP of the unaltered substrate (no reinforcing particles) has had little effect on the average hardness despite producing a refined grain structure within the processed zone. The retreating side of the processed zone demonstrates the most significant hardness increase over the substrate material. This correlates with the greatest quantity of reinforcing particles as indicated in Table 3. The WC-CoCr and Cr_3C_2-NiCr reinforced coatings exhibited an average hardness increase of approximately 540% and 500% respectively over the as-received AA5083. Addition of Al_2O_3 particles has resulted in a comparatively lower hardness increase to the MMC of 100%. This is attributed to the lower quantity of reinforcing particles present in the MMC and to the larger particle size of Al_2O_3. The measured increase in hardness is attributed to the micro-reinforcement mechanisms generated by the presence of the reinforcing particles. The superior hardness measured in the retreating side corresponds to an increase in wt.% of WC-CoCr material following the FSP (Table 3). This highlights the impact of the tool which has resulted in WC material being transported to the retreating side as opposed to being evenly distributed across the top surface of the coating layer.

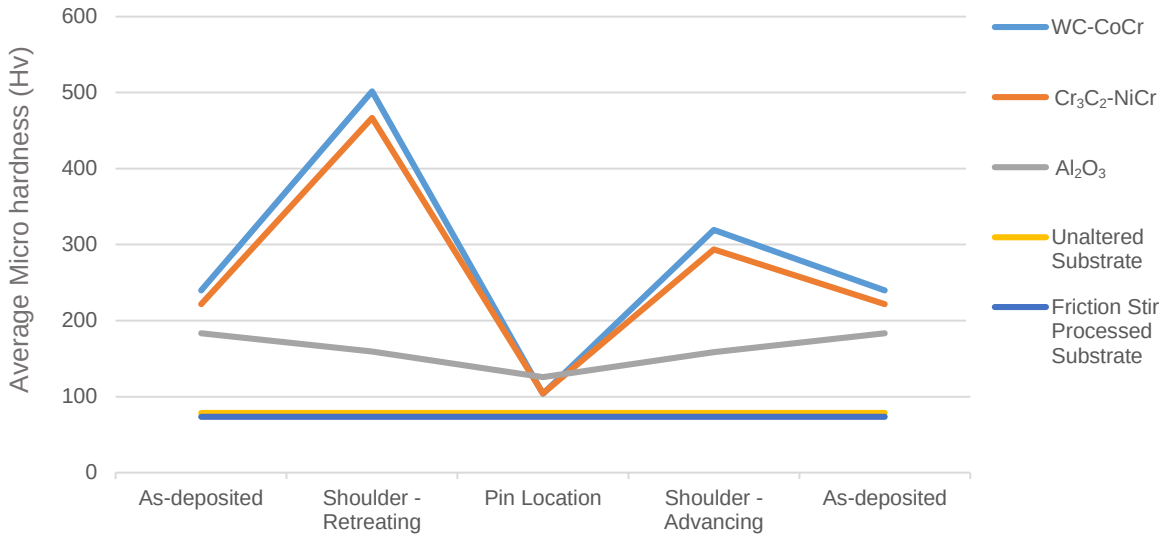

Fig 10. Average micro-hardness values with corresponding hardness indents on the WC-CoCr MMC.

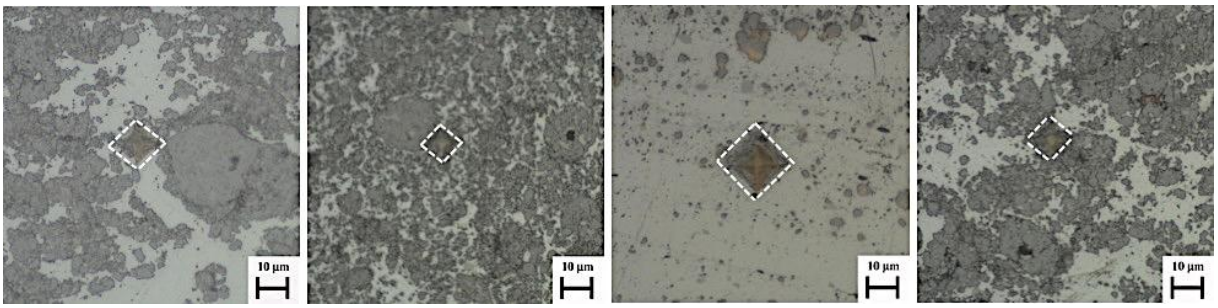

Fig. 11. Hardness indents showing the level of surrounding WC-CoCr particles [x500]. a) As-deposited; b) Retreating side; c) Pin location; d) advancing side.

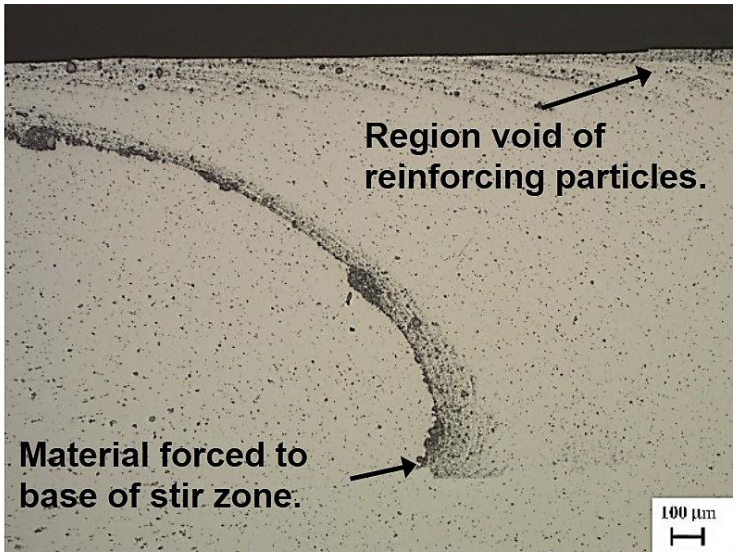

Fig 12. Light optical micrograph of reinforcing particles being pulled down from the surface [x50 unetched].

There have been a number of studies [16,17] that relate the hardness of an MMC to the distribution of reinforcing particles, specifically to the distance between particles (interparticle distance) within an MMC. Despite not directly examining hardness, Kouzeli et al. [18] developed a method to determine the interparticle distance by superimposing a number of lines of known length on to an optical micrograph of the material. The number of particle intercepts with the lines and the volume fraction of reinforcing particles was used to calculate the average interparticle distance [18]. This method is insensitive the dispersal quality of particles within an MMC, with agglomerated and evenly distributed particles yielding similar average interparticle distance values. As such, this method does not allow a suitable comparison to be made between MMCs containing evenly dispersed and agglomerated reinforcement particles. To address this, a number of studies [19–21] have investigated the generation of statistical models that are capable of quantifying the level of dispersion in MMCs. Khare et al. [19] developed a method that measures the free-space length which is defined as the width of the largest randomly placed square for which the average number of intersecting particles is zero. This method was applied to the MMC coatings in the as-deposited and SprayStirred conditions to highlight the variation in average interparticle distance. The results are presented in Table 4.

Table 4. Interparticle distance

Coating	WC-CoCr	Cr_3C_2-NiCr	Al_2O_3
Interparticle distance (µm) (as-deposited)	11.5	15.3	13.1
Interparticle distance (µm) (SprayStirred)	3.7	5.8	8.6
Reduction in interparticle distance (%)	68	60	34

The results show that, following FSP, the average interparticle spacing has dropped by 68% and 60% in the WC-CoCr and Cr_3C_2-NiCr coatings. FSP of Al_2O_3 resulted in a smaller drop in interparticle distance of 34%. Despite the variation in the level of reduction experienced by each respective coating, the results highlight the beneficial effects of subsequent FSP by showing a drop in the interparticle distance for all examined coatings.

4. CONCLUSIONS

WC-CoCr, Cr_3C_2-NiCr and Al_2O_3 powders have successfully been co-deposited with a metallic binder to produce particle reinforced MMC coatings. These coatings have subsequently been subjected to FSP, the aim of which was improve the distribution of reinforcing particles within the MMC matrix. Analysis of the coating microstructure was facilitated by light optical and

scanning electron microscopy techniques, as well as micro-hardness measurement. The following outlines the conclusions that can be drawn from this body of work.

- Micro-hardness measurements show that the WC-CoCr reinforced coating exhibited a hardness increase over the as-received AA5083 of approx. 70%, with the Cr_3C_2-NiCr and Al_2O_3 coatings demonstrating an increase of 60% and 55% respectively.
- The shearing forces generated by the FSP tool have resulted in substantial refinement of the agglomerates that are present in the as-deposited condition. The agglomerates have been refined to such an extent that their size was smaller than that of the original feedstock particles.
- Image analysis has indicated a reduction in the interparticle distance of all three coatings, with the WC-CoCr reinforced coating exhibiting a reduction of 65%.
- In the present study, reinforcing particles are forced towards the base of the stir zone as a consequence of the 2 mm pin. Hence, the centre of the stir zone was found to contain only minute quantities reinforcing particles. The minimal presence of reinforcements in this region has resulted in a comparably small (<20%) hardness increase over the unaltered substrate.
- In the case of the WC-CoCr reinforced MMC, FSP has resulted in approx. 120% increase in the average hardness over the as-deposited MMC. The measured hardness aligns with the interparticle distance, with coatings demonstrating the highest hardness (WC-CoCr) also presenting the smallest interparticle distance.

5. REFERENCES

[1] A. Papyrin, V. Kosarev, S. Klinkov, A. Alkhimov, V. Fomin, Cold Spray Technology, Elsevier, 2006.

[2] V.K. Champagne, The cold spray materials deposition process fundamentals and applications, 2007.

[3] L. Singh, V. Chawla, J.S. Grewal, A review on detonation gun sprayed coatings, J. Miner. Mater. Charact. Eng. 11 (2012) 243–265.

[4] K. Spencer, D.M. Fabijanic, M.X. Zhang, The use of Al-Al2O3 cold spray coatings to improve the surface properties of magnesium alloys, Surf. Coatings Technol. 204 (2009) 336–344.

[5] M. Yandouzi, E. Sansoucy, L. Ajdelsztajn, B. Jodoin, WC-based cermet coatings produced by cold gas dynamic and pulsed gas dynamic spraying processes, Surf. Coatings Technol. 202 (2007) 382–390.

[6] E.J.T. Pialago, C.W. Park, Cold spray deposition characteristics of mechanically alloyed Cu-CNT composite powders, Appl. Surf. Sci. 308 (2014) 63–74.

[7] D. Seo, M. Sayar, K. Ogawa, SiO 2 and MoSi 2 formation on Inconel 625 surface via SiC coating deposited by cold spray, Surf. Coatings Technol. 206 (2012) 2851–2858.

[8] H. Liao, B. Normand, C. Coddet, Influence of coating microstructure on the abrasive wear resistance of WC/Co cermet coatings, Surf. Coatings Technol. 124 (2000) 235–242.
[9] M. Couto, S. Dosta, M. Torrell, J. Fernández, J.M. Guilemany, Cold spray deposition of WC-17 and 12Co cermets onto aluminum, Surf. Coatings Technol. 235 (2013) 54–61.
[10] Y. Morisada, H. Fujii, T. Mizuno, G. Abe, T. Nagaoka, M. Fukusumi, Modification of thermally sprayed cemented carbide layer by friction stir processing, Surf. Coatings Technol. 204 (2010) 2459–2464.
[11] R. Miranda, J. Gandra, P. Vilaca, L. Quintino, T. Santos, Surface Modification by Solid State Processing, Woodhead Publishing Limited, 2008.
[12] Struers, Metallographic preparation of thermal spray coatings, 2014.
[13] J. Gandra, H. Krohn, R.M. Miranda, P. Vilaça, L. Quintino, J.F. Dos Santos, Friction surfacing - A review, J. Mater. Process. Technol. 214 (2014) 1062–1093.
[14] Z.Y. Ma, S.R. Sharma, R.S. Mishra, Effect of multiple-pass friction stir processing on microstructure and tensile properties of a cast aluminum-silicon alloy, Scr. Mater. 54 (2006) 1623–1626.
[15] B. Fiedler, F.H. Gojny, M.H.G. Wichmann, M.C.M. Nolte, K. Schulte, Fundamental aspects of nano-reinforced composites, Compos. Sci. Technol. 66 (2006) 3115–3125.
[16] D.A. Stewart, P.H. Shipway, D.G. McCartney, Abrasive wear behaviour of conventional and nanocomposite HVOF-sprayed WC–Co coatings, Wear. 225-229 (1999) 789–798.
[17] P.H. Shipway, D.G. McCartney, T. Sudaprasert, Sliding wear behaviour of conventional and nanostructured HVOF sprayed WC-Co coatings, Wear. 259 (2005) 820–827.
[18] M. Kouzeli, A. Mortensen, Size dependent strengthening in particle reinforced aluminium, 50 (2002) 39–51.
[19] H.S. Khare, D.L. Burris, A quantitative method for measuring nanocomposite dispersion, Polymer (Guildf). 51 (2010) 719–729.
[20] M. Yourdkhani, P. Hubert, Quantitative dispersion analysis of inclusions in polymer composites, ACS Appl. Mater. Interfaces. 5 (2013) 35–41.
[21] Z.P. Luo, J.H. Koo, Quantification of the layer dispersion degree in polymer layered silicate nanocomposites by transmission electron microscopy, Polymer (Guildf). 49 (2008) 1841–1852.